Back action evasion in optical lever detection

Shan Hao,[1] **Thomas P. Purdy,**[1,*]

[1] *Department of Physics and Astronomy, University of Pittsburgh, Pittsburgh, Pennsylvania 15260, USA*
[*] *tpp9@pitt.edu*

Abstract: The optical lever is a centuries old and widely-used detection technique employed in applications ranging from consumer products and industrial sensors to precision force microscopes used in scientific research. However, despite the long history, its quantum limits have yet to be explored. In general, any precision optical measurement is accompanied by optical force induced disturbance to the measured object (termed as back action) leading to a standard quantum limit (SQL). Here, we give a simple ray optics description of how such back action can be evaded in optical lever detection. We perform a proof-of-principle experiment demonstrating the mechanism of back action evasion in the classical regime, by developing a lens system that cancels extra tilting of the reflected light off a silicon nitride membrane mechanical resonator caused by laser-pointing-noise-induced optical torques. We achieve a readout noise floor two orders of magnitude lower than the SQL, corresponding to an effective optomechanical cooperativity of 100 without the need for an optical cavity. As the state-of-the-art ultra low dissipation optomechanical systems relevant for quantum sensing are rapidly approaching the level where quantum noise dominates, simple and widely applicable back action evading protocols will be crucial for pushing beyond quantum limits.

1. Introduction

Optical lever detection, which measures the angular deviation of light reflecting from a tilting surface, is among the oldest precision optical measurement techniques [1]. For multiple centuries, the technique has been widely employed in numerous applications ranging from consumer products [2, 3] and industrial sensors such as optical comparators to high precision scientific instruments such as atomic force microscopy(AFM) and its various variants, torsional balances for big-G measurement [4], and active mirror alignment for gravitational wave detectors [5, 6]. Although the optical lever is old and simple, contrary to general intuition, it is as sensitive as optical interferometry [7, 8], which has been more associated with precision measurement. However, the quantum limits of optical level detection have yet to be experimentally explored, as systems to date have been limited by thermal or other classical noise sources. Advances in nanomechanical resonators in the past few years [9–14] have pushed the device quality factor to a new level, reducing thermal noise, making quantum noise caused by optical forces (i.e., measurement back action) a dominant limit to be overcome. Here, we show that the effects of back action are evaded by modifying the optical lever beam path with a carefully designed lens system.

In optical lever detection, quantum measurement back action presents as noisy torques from random arriving photons (shot noise) recoiling off a device. The standard quantum limit (SQL) is the minimum noise achieved by balancing shot noise and its back action induced disturbance. Methods that sidestep this limit [15–17] are referred to as back action evasion. So far, the SQL and protocols for beating it have been extensively studied in interferometric optomechanical systems [18–20]. Surpassing the SQL will extend the scope and sensitivity of gravitational wave detectors [21] and enhance searches for dark matter candidates [22, 23] and tests of the validity of quantum mechanics at a macroscopic scale [24]. Most of the work done so far on back action evasion utilizes optical cavities to enhance optomechanical interaction strength. On the other hand, such cavities limit bandwidth, complicate the setup, and make systems prone to classical laser noise. One notable exception is recent work in levitated nanoparticle systems that approach the regime where back action can be evaded without using a cavity [25, 26].

The typical angular resolution for optical lever detection is on the order of $10\,\mathrm{prad}/\sqrt{\mathrm{Hz}}$ for applications such as AFMs [27, 28]. The technique has been pushed further with multiple bounces [29], non-classical laser sources such as single or multimode squeezed light [30, 31], and with cavity enhancement [32, 33]. However, these experiments are still far from the SQL. A method to surpass SQL was theoretically proposed only a few years ago by Enomoto, et al. [34]. Noise correlations introduced by the optomechanical interaction produce squeezing (sometimes referred to as ponderomotive squeezing) and can be used to evade back action in an optical lever detector, ultimately providing the resource for a quantum-enhanced measurement scheme capable of surpassing the SQL. We present a simple ray optics picture of this process and experimentally demonstrate this protocol for back action evasion at room temperature with classically driven laser noise. We observe an optomechanical cooperativity, which characterizes measurement strength relative to the SQL, up to 100. We also find that parameters needed for evading quantum back-action are within experimental reach. This quantum-enhanced optical lever detection protocol will be beneficial for ultra-high precision measurements such as AFM or scanning force microscopy utilizing high Q mechanical resonators [35], optical-tweezers-based sensors, and novel types of gravitational-wave detectors [36].

2. Quantum noise in optical lever

An optical lever, in itself, is very simple as shown in Fig. 1(a). In our system, a laser reflects off the node of a suspended membrane mechanical resonator. With the laser beam waist (w_0) much smaller than the mechanical wavelength (λ_m), the out-of-plane motion of the membrane at the node can be approximated as a tilting mirror. The deflection of the laser is then measured by a split photodetector, which takes the difference of the optical power on left and right sides. The precision of optical lever detection is limited by quantum noise, as photons strike the split photodetector randomly in time and with a spacial distribution following the beam intensity profile (represented by finite beam width in Fig. 1(a) and spread rays in Fig. 1(b)). This shot-noise-limited readout floor improves with laser power. Additionally, the random recoil of photons off the membrane imposes an imbalanced force noise, which tilts the mirror and redistributes the reflected photons. Such back action noise increases with laser power. The standard quantum limit resides where the sum of the two noise sources is at a minimum.

A simple case of back action evasion in an optical lever can be visualized in a ray optics picture as shown in Fig. 1(b). Uniformly distributed incoming rays reflect off a flat mirror and are focused through an output lens to its Fourier plane, P1 (red rays). Tilting of the mirror (blue line) by an external force displaces the focal point off the optical axis (blue rays). An incoming photon's beam path is described by a random incoming red ray. Such a single ray off the axis, produces a torque on the mirror proportional to the arm length. This torque causes a tilting of the mirror that gets larger when the ray is further from the pivot point, and the ray is consequently deflected further from the original reflection direction. Thus, the back-action-modified beam path for a given ray is equivalent to reflecting off a convex parabolic mirror (yellow line). In other words, the flat mirror effectively picks up a dynamical curvature due to optical back action forces. The deflected photons (yellow rays) converge back to the optical axis at a certain distance beyond P1. A split photodetector placed there sees no effects of back action, but retains sensitivity to the tilting of the mirror from external forces.

3. Gaussian optics picture

To better quantify the quantum noise, we decompose the optical field in the basis of Hermite-Gaussian (HG) modes, generalizing the treatment of [34]. In this section, we present the results of our calculations, which are detailed in the Appendix. We provide an analysis including the effect of higher order modes in Supplement 1. $U_{mn}(x, y, z)$ is the HG mode of order m in x

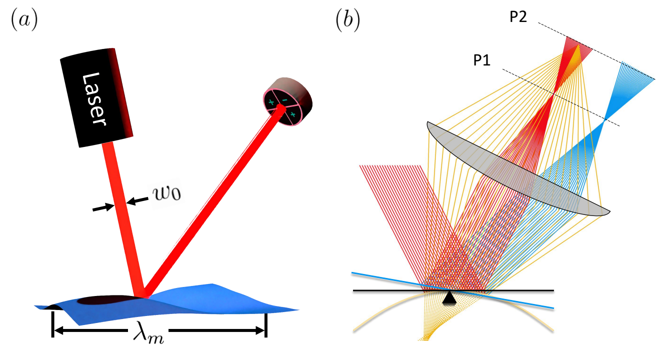

Fig. 1. (a) Optical lever detection of a membrane mechanical resonator. (b) Ray optics visualization of back action evasion in the low frequency limit. If the surface is fixed, the incoming red beams are reflected and focused by a lens to one point. If the mirror tilts due to external force, the rays will be focused to a different point (blue lines) on plane P1(Fourier plane). The yellow rays take account of the result of optical forces on the mirror. Rays impinging further from the pivot point give larger back action torques, and so the yellow rays appear to be reflected off a parabolic mirror and focused to plane P2, which we term back action evasion plane. The mirror curvature, and thus the location of P2, is frequency dependent following the mechanical response function. The maximum SNR sits between P1 and P2.

direction and n in y direction and propagating in z direction (see Supplement 1 Sec. S1.E for details). A laser in a coherent state of the U_{00} mode reflecting from an undulating surface can be thought of as scattering light into higher order HG modes. To first order, a small tilt of this Gaussian laser beam can be characterized as the addition of a U_{10} component with a small imaginary amplitude (in addition, small transverse displacements of the laser correspond to a real amplitude U_{10} component). This limit is relevant for our case where $w_0 \ll \lambda_m$ and the amplitude of motion of the membrane is small, and forms the basis of optical lever measurement.

In this case, the input field can be approximated as [37,38]

$$\hat{U}_{in} = \alpha U_{00}(x, y, z) + (d\hat{X}_1 + i d\hat{X}_2) U_{10}(x, y, z), \tag{1}$$

where $\alpha \gg 1$ is the coherent amplitude (neglecting quantum fluctuations in the fundamental mode, which do not contribute to the back action or measured signal in our experiment). $d\hat{X}_1$ and $d\hat{X}_2$ are vacuum amplitude and phase fluctuations of U_{10} that give rise to quantum limited beam displacement and pointing noise of the laser, respectively. The latter is responsible for readout noise at the detector, whereas the former seeds the mechanical back action on the membrane. The reflected field $\hat{U}_{out}$ can be associated with the input field $\hat{U}_{in}$ as (up to a change of direction of propagation)

$$\hat{U}_{out}(z = 0) = e^{-i2k\hat{\Phi}(x,y,t)} \hat{U}_{in}(z = 0),$$

where k is the laser wave number and $\hat{\Phi}(x, y, t)$ is the out-of-plane motion of the resonator. For a small beam waist, we can approximate $\hat{\Phi} \approx \hat{\beta}(t)x$, where $\hat{\beta}$ is the tilting angle of the surface of the membrane. $\hat{\beta}(\omega) \approx k_m \hat{X}(\omega) = k_m \chi_m(\omega)(\delta\hat{F}(\omega) + \hat{R}(\omega))$ has 2 sources, one generated by the thermal random force $\hat{R}(t)$ and the other generated by the optical force $\delta\hat{F}(t) \approx 2|\alpha|\hbar k k_m w_0 d\hat{X}_1$. Here $\hat{X}$ is the amplitude of motion and $\chi_m(\omega)$ is the mechanical response function. (See

Appendix for details.) The fluctuations on the output U_{10} mode are then given by:

$$d\hat{X}_1(\omega) \rightarrow d\hat{X}_1(\omega) \tag{2}$$

$$\begin{aligned} d\hat{X}_2(\omega) &\rightarrow d\hat{X}_2(\omega) - \alpha w_0 k \hat{\beta}(\omega) \\ &= d\hat{X}_2(\omega) + 2\hbar D \chi_m(\omega) \cdot d\hat{X}_1(\omega) + \sqrt{D}\chi_m(\omega)\hat{R}(\omega). \end{aligned} \tag{3}$$

Here $D = N|kk_m w_0|^2$. $N = |\alpha|^2$ is the photon flux, and $k_m = \frac{2\pi}{\lambda_m}$. In this process, the reflection due to back action induced tilting imprints the amplitude noise of U_{10} onto its phase quadrature. The generated correlation between amplitude and phase quadrature of the reflected beam is very similar to ponderomotive squeezing in cavity optomechanics [39–41] but different in that another spatial mode is put in a squeezed vacuum state as opposed to being bright squeezed.

The U_{00} mode does not contain information about the tilting of the membrane, but it acts as a local oscillator when weighted by the split photodetector step weighting function (±1 for two halves), allowing us to extract information about the tilting angle from the U_{10} mode. As the reflected beam propagates, the Gouy angle $\theta = \theta(z)$ generates a relative phase shift of θ between U_{00} and U_{10}. Thus, the Gouy angle is equivalent to the measured quadrature of U_{10}. (see Supplement 1 Sec. S1.G for details.) Picking a particular quadrature just requires putting the split photodetector at a specific location along the beam path, or adding lenses to adjust the Gouy phase.

Putting everything together, we can write down the expression for the power spectrum of the measured membrane tilting angle as

$$S_\beta = S_\beta^{Ba} + S_\beta^{Imp} + S_\beta^{Ba,Imp} + S_\beta^{Th} + S_\beta^{Detc}, \tag{4}$$

where $S_\beta^{Ba} = N\hbar^2 k^2 w_0^2 k_m^4 |\chi_m|^2$ is the back action of the laser on the membrane, $S_\beta^{Imp} = \frac{1}{4N w_0^2 k^2 \sin^2\theta}$ is the imprecision readout noise from the laser shot noise, S_β^{Th} is the thermal and zero point motion of the membrane, S_β^{Detc} counts for the loss of quantum efficiency in detection, and $S_\beta^{Ba,Imp} = \hbar k_m^2 \cot(\theta)\,\mathrm{Re}\{\chi_m\}$ is the interference term from the optomechanically induced correlation between the two quadratures described by Eq. (2) and Eq. (3) (see Supplement 1 Sec. S1.G for details). The minimum measurement noise (minimized over reflected power) that we can achieve neglecting the last three terms of Eq. (4) occurs at $\theta = \pi/2$ and represents the standard quantum limit for our system, $S_\beta^{SQL} = \hbar k_m^2 |\chi_m|$. Including the interference term, we find $S_\beta \geq \hbar k_m^2 \mathrm{Im}\{\chi_m\}$ (for all θ and reflected laser powers), which sets the Heisenberg limit. Over a particular range of Gouy phases the interference term can be made destructive and the SQL can be beaten. Measuring at the (frequency dependent) optimal value of θ provides an optimal detection basis of the superposition of the U_{00} and U_{10} modes.

4. Proof-of-principle experiment

At room temperature, thermal motion dominants over quantum back action for devices we currently have. To demonstrate the principle of back action evasion, we intentionally add classical laser displacement fluctuations Δx that are much larger than the quantum noise by modulating the laser spot position. In this case Eq. (4) becomes (see Appendix)

$$S_\beta = \frac{S_{\Delta x}/w_0^2}{N w_0^2 k^2 \sin^2\theta} |\cos\theta + 2\hbar D \chi_m \sin\theta|^2 + S_\beta^{th}. \tag{5}$$

where $S_{\Delta x}(\omega)$ is the spectrum of the classical laser position fluctuations, and we have neglected the quantum noise. As shown in Fig. 2, a commercially available (Norcada Inc.) silicon nitride (SiN) low stress (about 200 MPa) membrane (3.5 mm long, 1.5 mm wide and 100 nm thick) is clamped inside a vacuum chamber (1.3e-7 Torr) and positioned at the focal plane of the objective lens (f = 125 mm). An Acousto-Optic Modulator(AOM) is located at the other focal plane of the objective lens and is frequency modulated(FM) so that angular deviation of the 1st order diffracted beam is turned into laser (1064 nm) spot position modulation at the membrane. The reflected laser is then steered through an output lens (f = 125 mm) to a split photodetector that can move along the beam path to measure at different quadrature angles. The output lens maps the far field onto its Fourier plane, generating additional accumulated Gouy phase [42](also see Supplement 1 Sec. S1.F for details) allowing us to access all quadratures with finite movement of the split photodetector. Near the Fourier plane, the split photodetector is insensitive to the injected noise, but sensitive to the vibrations of the membrane.

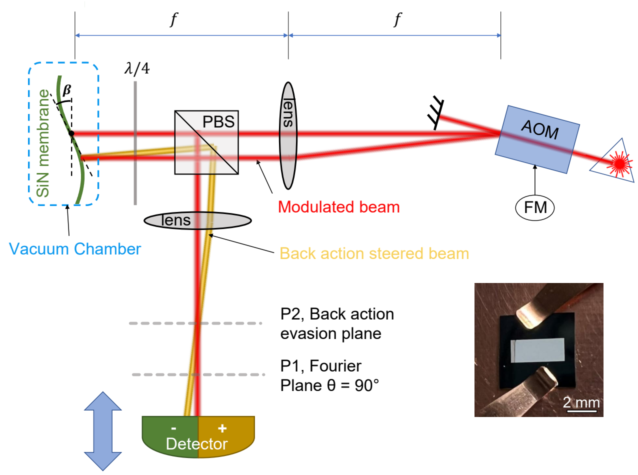

Fig. 2. An FM modulated AOM is placed at one focal plane of the input lens and the SiN membrane is at the other, so that the angular modulation of the first order diffracted beam turns into position modulation at the plane of the device. The modulated beam disturbs the motion of the membrane and deflects itself into a different direction (yellow). The illustrated case corresponds to a modulation frequency higher than the mechanical resonance frequency, so that the mechanical response lags 180° behind the modulated force, leading to the reflected beam being steered toward the undisplaced beam and putting the back action evasion plane P2 before P1. Inset: SiN membrane device.

We modulate the laser spot position by chirping (which plays the role of classical noise) the AOM FM frequency across the resonance of the mechanical mode of interest ($f_m \approx 371$kHz). The resultant driven motion is much larger than the thermal motion. Then we measure the spectral response of the tilting angle at different quadrature angles($S_\beta(\theta)$) by translating the split photodetector along the beam path near the Fourier plane and averaging at each quadrature angle for longer than the decay time of the mode (see Supplement 1 Sec. S2.G for details).

A density plot of the measured spectra against quadrature angles is shown in Fig. 3(b). We calculate the corresponding theoretical density plot (Fig. 3(a)) from Eq. (5) based on independently measured experimental parameters. To visualize the spectra $S_\beta(\theta)$, we normalize to the measured background noise floor $S_\beta^{Cla}(\theta) = \frac{S_{\Delta x}/w_0^2}{N w_0^2 k^2} \cot^2\theta$, i.e., the projection of the classical injected noise to the measured quadrature. Such normalization mimics that of the spectrum to laser shot noise in the case of quantum back action evasion, by considering our classical injected noise as artificially enlarged quantum amplitude fluctuations. In the case of pure quantum noise, the shot-noise-limited phase quadrature fluctuations would contribute a significant imprecision background to the overall signal, creating a quadrature-independent background level. The region

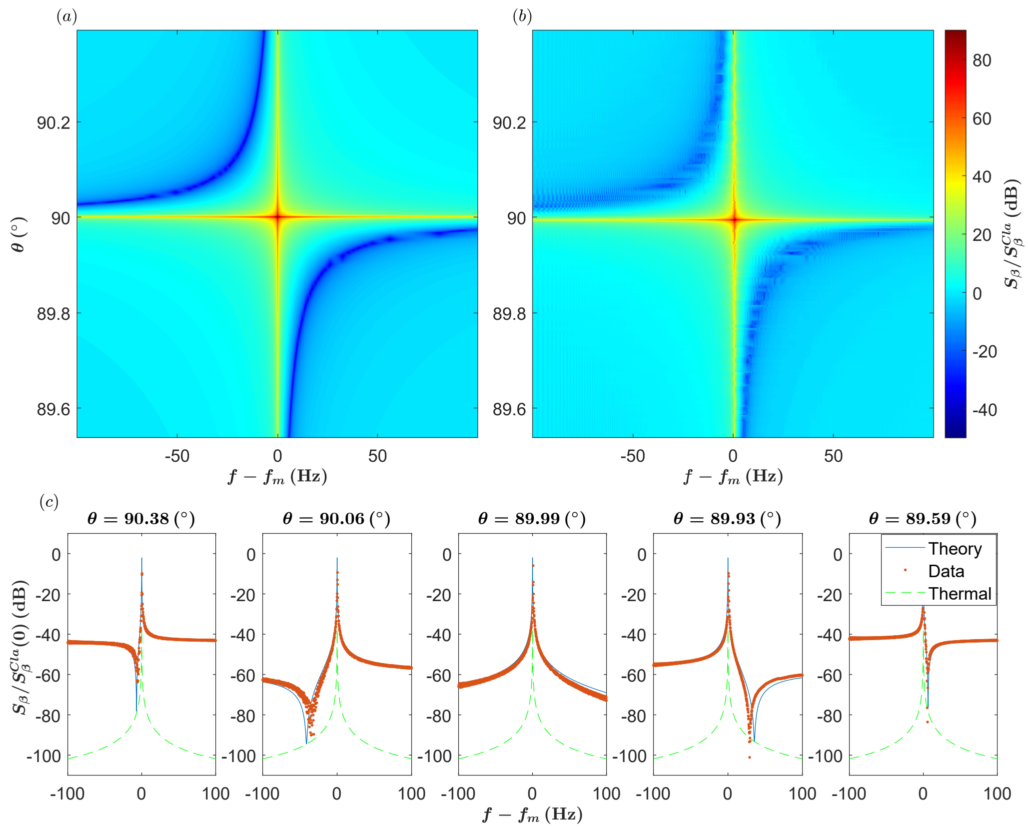

Fig. 3. (a) Zero free parameter theoretical expectation of S_β normalized to injected noise at corresponding quadrature angle $S_\beta^{Cla}(\theta)$ versus quadrature angles and frequencies. (b) Corresponding experiment data. Mode frequency $f_m = 371$ kHz, $Q = 3.2 \times 10^6$, $m_{eff} = 4.06 \times 10^{-10}$ kg, $T = 297.5$ K and the laser power $P = 21$ mW. Observation of region with less than 0 dB demonstrates the interference mechanism of back action evasion in optical lever detection. (c) Expectation and experimental data of S_β at several representative quadrature angles θ normalized to input noise $S_\beta^{Cla}(\theta = 0)$. The curves can be interpreted as the gain function at different quadrature angles. The green dashed curves mark the thermal motion level, which stops dips from going deeper and demonstrates our ability to resolve small motion on top of the large injected noise. Due to the sub-Hz resonance frequency random drift which is beyond our active control capability, the sharp peaks and dips are blurred by random resonance frequency drift.

below 0 dB is where the perceived motion spectrum is smaller than the artificially injected noise floor, a classical equivalent of ponderomotive squeezing.

Figure 3(c) are several spectra from the same data set at some representative quadrature angles. These spectra are normalized to the input noise $S_\beta^{Cla}(\theta = 0°)$. The curves can thus be interpreted as the gain function of the system with the peak of the motion approaching 0 dB, corresponding to a measured cooperativity close to 1. Zero free parameter theoretical expectations are shown as solid blue lines to have excellent qualitative agreement with experiment data. At 90°, the curve is just the Lorentzian of the classical noise driven motion of the mechanical mode with no back action evasion, equivalent to what will be measured in the far field. At other quadrature angles, the destructive interference (the dips in the curves) of injected noise and its driven motion emerges in a frequency and quadrature dependent fashion, demonstrating the mechanism of back action evasion in optical lever detection. Green dashed lines are the expected thermal motion spectrum, which stops the back action evasion dips from reaching deeper, and demonstrates our ability to resolve small motion on top of the large classical injected noise.

5. Cooperativity in optical lever

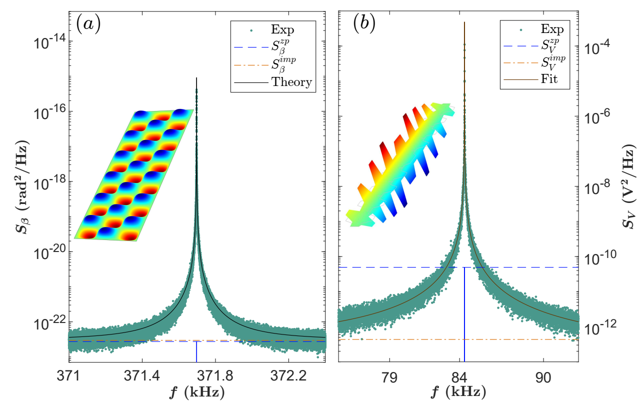

Fig. 4. (a) Room temperature thermal motion PSD of the membrane device inspected in back action experiment. The laser power is instead $P = 27.2$ mW. The green dots are experimental data averaged for over 30 minutes. Black is the zero free parameter calculation. The blue dashed line marks the peak of zero point motion of the device, which is $5.23\,\mathrm{prad}/\sqrt{\mathrm{Hz}}$. The orange dash-dotted line marks the measured imprecision noise level, which is $5.45\,\mathrm{prad}/\sqrt{\mathrm{Hz}}$, slightly above the zero point motion. (b) Thermal motion PSD (as signal V measured by a split photodetector) of a SiN phononic crystal string of $f_m \approx 84$ kHz, $Q \approx 1.0 \times 10^5$ and $m_{eff} \approx 7.3 \times 10^{-13}$ kg at $T = 20$ K. A Lorentzian fit yield the cooperativity to be approximately $C \approx 100$. Insets show mode shapes from simulation.

Quantum back action evasion requires large optomechanical coopperativity, C. For an ideal measurement, a cooperativity of 1 indicates the ability to resolve signals at the scale of the zero point motion and the regime where the back action induced motion becomes comparable to the zero point motion. For $C > 1$, the signal from back action induced motion dominated over the shot noise floor. For $C > n_{th}$, (where n_{th} is the average thermal occupation of the mechanical resonator) the back action induced motion becomes larger than the thermal motion and limits measurement sensitivity. Calculated from the signal-to-noise ratio (SNR) of zero point motion to shot noise limited readout floor, the explicit form of the effective cooperativity for a mechanical membrane or string of sinusoidal mode shape and under small beam waist approximation can be written as

$$C = \frac{2PQ}{m_{eff}} \frac{k w_0^2 k_m^2}{c \omega_m^2}, \tag{6}$$

where P is the laser power reflected from the device, Q is the mode quality factor, m_{eff} is the effective mass of the mode, and ω_m is the mechanical mode angular frequency.

Figure 4(a) shows the measured thermal motion spectrum of the mode probed in the back action evasion experiment. The zero-point motion spectrum, S_β^{zp}, is at the same level as S_β^{imp}. From Eq. (6) and with the measured experiment parameters, we estimate the cooperativity to be $C \approx 2$. Given the estimated net quantum efficiency $\eta \approx 21\%$ (including geometrical factors [43–45] and optical losses) (see Supplement 1 Sec. S2.B for details), our measured SNR of the thermal motion spectrum (peak to noise floor) is consistent with the theoretical expectation (SNR = $4\eta n_{th}C$).

The theory curves in Fig. 4 have already taken into account the quantum efficiency (also for theory curves in Fig. 3), and agree very well with experiment data. To illustrate the achievability of large cooperativity in an optical lever system and to push the experiment toward quantum back action evasion, we measure the thermal motion power spectrum density (PSD) of a SiN phononic crystal string [9] (about 2 mm long, 10 μm wide and 120 nm thick) fundamental torsional mode with laser of power $P = 12.2$ mW focused to a beam waist $w_0 = 4$ μm at $T = 20$ K (see Supplement 1 Sec. S2.H for details)), as shown in Fig. 4(b). Using Q measured from ring down, we fit the Lorentzian PSD and estimate the cooperativity to be around $C \approx 100$. Compared to the membrane, the cooperativity of the string is much higher due to its smaller effective mass m_{eff}. We also note a recent report [14] of higher SNR for torsional mode with wider strings of much higher Q.

6. Outlook

We finally consider the experimental prospects for implementing the optical lever back action evading protocol in the quantum regime, where it can be utilized to beat the SQL. To observe quantum back action evasion, we will need the cooperativity to be larger than the thermal occupation. This is possible with parameters available from state-of-the-art optomechanical string devices. With phononic crystal shielding, soft clamping [46, 47], and dissipation dilution [9, 14], quality factors can exceed $Q > 10^9$. Moreover, the effective masses m_{eff} of these string devices are much smaller than those of membranes. Strained crystalline materials such as Si [48] or SiC [10] can have still lower dissipation at cryogenic temperature. Soft-clamped, 2D membrane resonators have better laser power handling and have been demonstrated to have comparable quality factors as that of strings [12, 49]. Such state-of-the-art mechanical resonators can increase cooperativity by several orders of magnitude, potentially pushing it above the thermal occupation. On the optical side, photonic crystal mirrors can be implemented in string or membrane resonators to push reflectivity close to unity [50, 51] increasing the reflected laser power and potentially incorporating multiple bounces [29] to further enhance the per-photon interaction strength. Such high reflectivity resonators can also be incorporated as one mirror in an optical cavity with a specially tailored transverse mode spectrum in order to resonantly enhance the cooperativity [52] by another few orders, leaving considerable parameter space to deal with experimental imperfections and laser heating. With these improvements, quantum back action will be the dominant noise at cryogenic temperature, but can now be readily dealt with.

Funding. NSF foundation Award No.2047823 and Charles E. Kaufman foundation.

Acknowledgments. We thank Robinjeet Singh for fabricating our string mechanical resonator at the NIST Center for Nanoscale Science and Technology.

Disclosures. The authors declare no conflicts of interest.

Data availability. Data underlying the results presented in this paper are not publicly available at this time but may be obtained from the authors upon reasonable request.

Supplemental document. See Supplement 1 for supporting content.

References

1. R. V. Jones, "Some developments and applications of the optical lever," J. Sci. Instruments **38**, 37–45 (1961).
2. C. C. Hsiao, C. Y. Peng, and T. S. Liu, "An optical lever approach to photodetector measurements of the pickup-head flying height in an optical disk drive," Meas. Sci. Technol. **17**, 2335–2342 (2006).
3. F. W. Cuomo, "Theory and applications of optical fiber lever sensors," Nasa contractor report, cr-185344 (1989).
4. C. Rothleitner and S. Schlamminger, "Invited review article: Measurements of the newtonian constant of gravitation, g," Rev. Sci. Instruments **88**, 111101 (2017).

5. E. Hirose, K. Kawabe, D. Sigg, R. Adhikari, and P. R. Saulson, “Angular instability due to radiation pressure in the ligo gravitational-wave detector,” Appl. Opt. **49**, 3474–3484 (2010).
6. K. Kokeyama, J. G. Park, K. Cho, S. Kirii, T. Akutsu, M. Nakano, S. Kambara, K. Hasegawa, N. Ohishi, K. Doi, and S. Kawamura, “Demonstration for a two-axis interferometric tilt sensor in kagra,” Phys. Lett. A **382**, 1950–1955 (2018).
7. C. A. J. Putman, B. G. de Grooth, N. F. van Hulst, and J. Greve, “A theoretical comparison between interferometric and optical beam deflection technique for the measurement of cantilever displacement in afm,” Ultramicroscopy **42-44**, 1509–1513 (1992).
8. S. M. Barnett, C. Fabre, and A. Maıtre, “Ultimate quantum limits for resolution of beam displacements,” The Eur. Phys. J. D - At. Mol. Opt. Plasma Phys. **22**, 513–519 (2003).
9. A. H. Ghadimi, S. A. Fedorov, N. J. Engelsen, M. J. Bereyhi, R. Schilling, D. J. Wilson, and T. J. Kippenberg, “Elastic strain engineering for ultralow mechanical dissipation,” Science **360**, 764–768 (2018).
10. E. Romero, V. M. Valenzuela, A. R. Kermany, L. Sementilli, F. Iacopi, and W. P. Bowen, “Engineering the dissipation of crystalline micromechanical resonators,” Phys. Rev. Appl. **13**, 044007 (2020).
11. M. J. Bereyhi, A. Beccari, R. Groth, S. A. Fedorov, A. Arabmoheghi, T. J. Kippenberg, and N. J. Engelsen, “Hierarchical tensile structures with ultralow mechanical dissipation,” Nat. Commun. **13**, 3097 (2022).
12. Y. Tsaturyan, A. Barg, E. S. Polzik, and A. Schliesser, “Ultracoherent nanomechanical resonators via soft clamping and dissipation dilution,” Nat. Nanotechnol. **12**, 776–783 (2017).
13. G. S. MacCabe, H. Ren, J. Luo, J. D. Cohen, H. Zhou, A. Sipahigil, M. Mirhosseini, and O. Painter, “Nano-acoustic resonator with ultralong phonon lifetime,” Science **370**, 840–843 (2020).
14. J. R. Pratt, A. R. Agrawal, C. A. Condos, C. M. Pluchar, S. Schlamminger, and D. J. Wilson, “Nanoscale torsional dissipation dilution for quantum experiments and precision measurement,” Phys. Rev. X **13**, 011018 (2023).
15. V. B. Braginsky, F. Y. Khalili, and K. S. Thorne, *Quantum Measurement* (Cambridge University Press, Cambridge, 1992).
16. H. J. Kimble, Y. Levin, A. B. Matsko, K. S. Thorne, and S. P. Vyatchanin, “Conversion of conventional gravitational-wave interferometers into quantum nondemolition interferometers by modifying their input and/or output optics,” Phys. Rev. D **65**, 022002 (2001).
17. A. A. Clerk, M. H. Devoret, S. M. Girvin, F. Marquardt, and R. J. Schoelkopf, “Introduction to quantum noise, measurement, and amplification,” Rev. Mod. Phys. **82**, 1155–1208 (2010).
18. J. Suh, A. J. Weinstein, C. U. Lei, E. E. Wollman, S. K. Steinke, P. Meystre, A. A. Clerk, and K. C. Schwab, “Mechanically detecting and avoiding the quantum fluctuations of a microwave field,” Science **344**, 1262–1265 (2014).
19. D. Mason, J. Chen, M. Rossi, Y. Tsaturyan, and A. Schliesser, “Continuous force and displacement measurement below the standard quantum limit,” Nat. Phys. **15**, 745–749 (2019).
20. H. Yu *et al.*, “Quantum correlations between light and the kilogram-mass mirrors of ligo,” Nature **583**, 43–47 (2020).
21. B. P. Abbott *et al.*, “Observation of gravitational waves from a binary black hole merger,” Phys. Rev. Lett. **116**, 061102 (2016).
22. D. Carney, S. Ghosh, G. Krnjaic, and J. M. Taylor, “Proposal for gravitational direct detection of dark matter,” Phys. Rev. D **102**, 072003 (2020).
23. D. Carney *et al.*, “Mechanical quantum sensing in the search for dark matter,” Quantum Sci. Technol. **6**, 024002 (2021).
24. M. Carlesso, S. Donadi, L. Ferialdi, M. Paternostro, H. Ulbricht, and A. Bassi, “Present status and future challenges of non-interferometric tests of collapse models,” Nat. Phys. **18**, 243–250 (2022).
25. A. Militaru, M. Rossi, F. Tebbenjohanns, O. Romero-Isart, M. Frimmer, and L. Novotny, “Ponderomotive squeezing of light by a levitated nanoparticle in free space,” Phys. Rev. Lett. **129**, 053602 (2022).
26. L. Magrini, V. A. Camarena-Chávez, C. Bach, A. Johnson, and M. Aspelmeyer, “Squeezed light from a levitated nanoparticle at room temperature,” Phys. Rev. Lett. **129**, 053601 (2022).
27. S. Alexander, L. Hellemans, O. Marti, J. Schneir, V. Elings, P. K. Hansma, M. Longmire, and J. Gurley, “An atomic-resolution atomic-force microscope implemented using an optical lever,” J. Appl. Phys. **65**, 164–167 (1989).
28. G. Meyer and N. M. Amer, “Novel optical approach to atomic force microscopy,” Appl. Phys. Lett. **53**, 1045–1047 (1988).
29. J. M. Hogan, J. Hammer, S. W. Chiow, S. Dickerson, D. M. S. Johnson, T. Kovachy, A. Sugarbaker, and M. A. Kasevich, “Precision angle sensor using an optical lever inside a sagnac interferometer,” Opt. Lett. **36**, 1698–1700 (2011).
30. N. Treps, N. Grosse, P. Bowen Warwick, C. Fabre, A. Bachor Hans, and K. Lam Ping, “A quantum laser pointer,” Science **301**, 940–943 (2003).
31. R. C. Pooser and B. Lawrie, “Ultrasensitive measurement of microcantilever displacement below the shot-noise limit,” Optica **2**, 393–399 (2015).
32. K. Komori, Y. Enomoto, C. P. Ooi, Y. Miyazaki, N. Matsumoto, V. Sudhir, Y. Michimura, and M. Ando, “Attonewton-meter torque sensing with a macroscopic optomechanical torsion pendulum,” Phys. Rev. A **101**, 011802(R) (2020).
33. T. Shimoda, Y. Miyazaki, Y. Enomoto, K. Nagano, and M. Ando, “Coherent angular signal amplification using an optical cavity,” Appl. Opt. **61**, 3901–3911 (2022).
34. Y. Enomoto, K. Nagano, and S. Kawamura, “Standard quantum limit of angular motion of a suspended mirror and

homodyne detection of a ponderomotively squeezed vacuum field," Phys. Rev. A **94**, 012115 (2016).
35. D. Halg, T. Gisler, Y. Tsaturyan, L. Catalini, U. Grob, M.-D. Krass, M. Heritier, H. Mattiat, A.-K. Thamm, R. Schirhagl, E. C. Langman, A. Schliesser, C. L. Degen, and A. Eichler, "Membrane-based scanning force microscopy," Phys. Rev. Appl. **15**, L021001 (2021).
36. M. Ando, K. Ishidoshiro, K. Yamamoto, K. Yagi, W. Kokuyama, K. Tsubono, and A. Takamori, "Torsion-bar antenna for low-frequency gravitational-wave observations," Phys. Rev. Lett. **105**, 161101 (2010).
37. E. Morrison, B. J. Meers, D. I. Robertson, and H. Ward, "Automatic alignment of optical interferometers," Appl. Opt. **33**, 5041–5049 (1994).
38. A. Wünsche, "Quantization of gauss–hermite and gauss–laguerre beams in free space," J. Opt. B: Quantum Semiclassical Opt. **6**, S47–S59 (2004).
39. D. W. C. Brooks, T. Botter, S. Schreppler, T. P. Purdy, N. Brahms, and D. M. Stamper-Kurn, "Non-classical light generated by quantum-noise-driven cavity optomechanics," Nature **488**, 476–480 (2012).
40. T. P. Purdy, P. L. Yu, R. W. Peterson, N. S. Kampel, and C. A. Regal, "Strong optomechanical squeezing of light," Phys. Rev. X **3**, 031012 (2013).
41. A. H. Safavi-Naeini, S. Gröblacher, J. T. Hill, J. Chan, M. Aspelmeyer, and O. Painter, "Squeezed light from a silicon micromechanical resonator," Nature **500**, 185–189 (2013).
42. M. F. Erden and H. M. Ozaktas, "Accumulated gouy phase shift in gaussian beam propagation through first-order optical systems," J. Opt. Soc. Am. A **14**, 2190–2194 (1997).
43. N. Treps, U. Andersen, B. Buchler, P. K. Lam, A. Maitre, H. A. Bachor, and C. Fabre, "Surpassing the standard quantum limit for optical imaging using nonclassical multimode light," Phys. Rev. Lett. **88**, 203601 (2002).
44. G. C. Knee and W. J. Munro, "Fisher information versus signal-to-noise ratio for a split detector," Phys. Rev. A **92**, 012130 (2015).
45. S. P. Walborn, G. H. Aguilar, P. L. Saldanha, L. Davidovich, and R. L. d. Filho, "Interferometric sensing of the tilt angle of a gaussian beam," Phys. Rev. Res. **2**, 033191 (2020).
46. S. A. Fedorov, A. Beccari, N. J. Engelsen, and T. J. Kippenberg, "Fractal-like mechanical resonators with a soft-clamped fundamental mode," Phys. Rev. Lett. **124**, 025502 (2020).
47. M. J. Bereyhi, A. Arabmoheghi, A. Beccari, S. A. Fedorov, G. Huang, T. J. Kippenberg, and N. J. Engelsen, "Perimeter modes of nanomechanical resonators exhibit quality factors exceeding 10^9 at room temperature," Phys. Rev. X **12**, 021036 (2022).
48. A. Beccari, D. A. Visani, S. A. Fedorov, M. J. Bereyhi, V. Boureau, N. J. Engelsen, and T. J. Kippenberg, "Strained crystalline nanomechanical resonators with quality factors above 10 billion," Nat. Phys. **18**, 436–441 (2022).
49. D. Shin, A. Cupertino, M. H. J. de Jong, P. G. Steeneken, M. A. Bessa, and R. A. Norte, "Spiderweb nanomechanical resonators via bayesian optimization: Inspired by nature and guided by machine learning," Adv. Mater. **34**, 2106248 (2022).
50. U. Kemiktarak, M. Durand, M. Metcalfe, and J. Lawall, "Cavity optomechanics with sub-wavelength grating mirrors," New J. Phys. **14**, 125010 (2012).
51. R. A. Norte, J. P. Moura, and S. Groblacher, "Mechanical resonators for quantum optomechanics experiments at room temperature," Phys. Rev. Lett. **116**, 147202 (2016).
52. T. Shimoda, Y. Miyazaki, Y. Enomoto, K. Nagano, and M. Ando, "Coherent angular signal amplification using an optical cavity," Appl. Opt. **61**, 3901–3911 (2022).
53. A. E. Siegman, *Lasers* (University Science Books, 1986).
54. M. Pinard, Y. Hadjar, and A. Heidmann, "Effective mass in quantum effects of radiation pressure," The Eur. Phys. J. D - At. Mol. Opt. Plasma Phys. **7**, 107–116 (1999).

Appendix

Here, we calculate the expected photodetection signal for our system under the small beam waist approximation. See the supplement for additional details and a discussion of the effects of a large beam waist. The input field of a typical laser of power P in the frame rotating at laser frequency ω_L can be written in the basis of Hermite-Gaussian(HG) modes as

$$\alpha U_{00} + \sum_{mn} \hat{\delta}_{mn} U_{mn}.$$

Here $U_{mn}(x, y, z)$ are mth order in x and nth order in y HG mode functions for modes propagating along z and focused to waist w_0 at $z = 0$ where membrane is located (see the Supplement S1.D for detailed definition of HG beam). $|\alpha|^2 = N = \frac{P}{\hbar\omega_L}$ and α is assumed to be real without loss of generality, and $\hat{\delta}_{mn}$ represents the vacuum fluctuation in U_{mn}. $\hat{\delta}_{mn} = d\hat{X}_1^{mn} + i d\hat{X}_2^{mn}$ are quantum Langevin noise operators where $d\hat{X}_1^{mn}$ is the amplitude vacuum fluctuation, $d\hat{X}_2^{mn}$ is the phase vacuum fluctuation and $\langle d\hat{X}_i^{mn}(\omega)(d\hat{X}_j^{pq}(\omega'))^\dagger\rangle = \frac{1}{4}\delta_{ij}\delta_{mp}\delta_{nq}\delta(\omega - \omega')$

The reflection of the laser field off the device can be calculated with Fourier optics. The reflected field $\hat{U}_{out}$ can be associated with the input field $\hat{U}_{in}$ as (up to a change of direction of propagation)

$$\hat{U}_{out}(z=0) = \hat{U}_{in} e^{-i2k\hat{\Phi}(x,y,t)},$$

where $k = \frac{\omega_L}{c}$, $\hat{\Phi}(x,y,t) = \hat{X}(t)\phi(x,y)$, where $\hat{X}$ is the amplitude of motion and $\phi(x,y) = \sin(\frac{l\pi}{a}(x-\frac{a}{2}))\sin(\frac{p\pi}{b}(y-\frac{b}{2}))$ is the out-of-plane motion mode shape (origin put at the center of the membrane, a and b are membrane side lengths, and l and p are mechanical mode indices) and can be approximated to $\hat{\Phi}(x,y,t) \approx \hat{X}(t)k_m x$ as the laser beam waist is much smaller than the mechanical wave length ($w_0 \ll \frac{2\pi}{k_m}$, k_m is mechanical wave numbers) and centered to the anti-node in y direction and the node in the x direction (center of the membrane). $\hat{X}(t)$ satisfy the equation of motion,

$$m_{eff}\ddot{\hat{X}} + m_{eff}\Gamma\dot{\hat{X}} + m_{eff}\omega_m^2\hat{X} = \hat{F},$$

where $\hat{F}$ is the force acting on the membrane and Γ is the damping rate. In the frequency space

$$\hat{X}(\omega) = \chi_m(\omega)\hat{F}(\omega), \tag{7}$$

where $\chi_m(\omega) = \frac{1}{m_{eff}}\frac{1}{(\omega_m^2-\omega^2)+i\omega\Gamma}$.

With the approximation made above, we have

$$\begin{aligned}\hat{U}_{out}(z=0) &\approx \hat{U}_{in}(1 - i2k\hat{X}(t)k_m x) \\ &\approx (\alpha U_{00} + \sum_{mn}\hat{\delta}_{mn}U_{mn})(1 - i2k\hat{\beta}(t)x) \\ &\approx \alpha U_{00} + (d\hat{X}_1^{10} + i(d\hat{X}_2^{10} - \alpha w_0 k\hat{\beta}(t)))U_{10} \\ &+ \sum_{mn\neq 10}\hat{\delta}_{mn}U_{mn},\end{aligned}$$

where we have used the fact that $\frac{2}{w_0}xU_{00} = U_{10}$ and $\hat{\beta}(t) \equiv \hat{X}(t)k_m$ is the tilting angle at the node.

Propagating the reflected field out, we have the light field at distance as:

$$\begin{aligned}\hat{U}_{out}(z) &= \alpha U_{00}(x,y,z) \\ &+ (d\hat{X}_1^{10} + i(d\hat{X}_2^{10} - \alpha w_0 k\hat{\beta}(t)))U_{10}(x,y,z) \\ &+ \sum_{mn\neq 10}\hat{\delta}_{mn}U_{mn}(x,y,z),\end{aligned}$$

The signal $V(t)$ for the split photodetector at z is proportional to

$$\begin{aligned}\hat{V}(t) \propto &\int_{-\infty}^{0}dx\int_{-\infty}^{\infty}dy|\hat{U}_{out}(x,y,z)|^2 \\ &- \int_{0}^{\infty}dx\int_{-\infty}^{\infty}dy|\hat{U}_{out}(x,y,z)|^2.\end{aligned}$$

Taking into account that there is a relative phase shift among U_{mn} due to Gouy phase, we have (the spectrum of $\hat{V}(t)$ is normalized to the shot noise floor, assuming $\alpha \gg 1$)

$$\begin{aligned}\hat{V}(t) \approx\ &2F_{00,10}[d\hat{X}_1^{10}\cos\theta_a - (d\hat{X}_2^{10} - \alpha w_0 k\hat{\beta})\sin\theta_a] \\ &+ 2\sum_{mn\neq 10}(d\hat{X}_1^{mn}\cos\theta_a - d\hat{X}_2^{mn}\sin\theta_a)F_{00,mn},\end{aligned}$$

where $F_{lm,pq} = \iint dxdyU_{lm}(z=0)U^*_{pq}(z=0)F_{weight}$ and F_{weight} for split detector is simply ± 1 for left and right half plane.

In actual experiment, the light goes through a lens system. The propagation can be done with the help of ABCD matrices [53]. However, Gouy angle calculated this way does not yield the correct phase differences between HG modes. Here, we have replaced Gouy angle θ with accumulated Gouy angle θ_a to correctly count for the phase differences between HG modes in lens system [42]. Under the thin lens approximation the beam curvature get modified but beam waist and phase remain the same which makes the Gouy phase fail to describe relative phase difference between HG modes. The accumulated Gouy phase is calculated by summing up the Gouy phase change during free space propagation between the lenses. In the main text, we just use symbol θ for simplicity.

The tilting angle $\hat{\beta}$ has 2 sources, one generated by the thermal random force $\hat{R}(t)$ and the other generated by the optical force $\delta\hat{F}(t)$. When the laser strikes the node of the membrane, because of the vacuum amplitude fluctuation $d\hat{X}_1^{10}$, the membrane experience a fluctuating force [54](assuming $\alpha \gg 1$)

$$\delta\hat{F}(t) \approx 2\hbar k \iint dxdy|\hat{U}_{in}|^2\phi(x,y) = 4\hbar k|\alpha|C_{00,10}d\hat{X}_1^{10},$$

where $C_{lm,pq} \equiv \int U_{lm}(z=0)U^*_{pq}(z=0)\phi(x,y)dxdy$, which under small laser beam waist approximation is evaluated to $C_{00,10} = \frac{k_m w_0}{2}$. Then from Eq. (7),

$$\hat{X}(\omega) = \chi_m(\omega)(\delta\hat{F}(\omega) + \hat{R}(\omega)),$$

and the spectral density of the split photodetector can be calculated to be

$$\begin{aligned} S_V(f) = {} & F^2_{00,10}(\sin^2\theta_a + |\cos\theta_a + 2\hbar D\chi_m \sin\theta_a|^2) \\ & + \sum_{mn\neq 10} F^2_{00,mn} + F^2_{00,10}|2\alpha w_0 k \sin\theta_a|^2 S^{th}_\beta(f) \end{aligned}$$

where $S^{th}_\beta(f) = 2|k_m\chi_m|^2 m_{eff}\Gamma k_b T$ (assuming $k_b T \gg \hbar\omega_m$), $S^{zp}_\beta(f) = |k_m\chi_m|^2 m_{eff}\Gamma\hbar\omega_m$ and $D = |kk_m w_0\alpha|^2$. The tilt angle spectral density follows as

$$\begin{aligned} S_\beta(f) = {} & \frac{1}{4Nw_0^2k^2\sin^2\theta_a} + N\hbar^2k^2w_0^2k_m^4|\chi_m|^2 + S^{th}_\beta(f) \\ & + \hbar k_m^2 \mathrm{Re}\{\chi_m\}\cot\theta_a + \frac{1}{4Nw_0^2k^2\sin^2\theta_a}\sum_{mn\neq 10}\frac{F^2_{00,mn}}{F^2_{00,10}}. \end{aligned}$$

Assuming negligible thermal motion $S^{th}_\beta(f) \approx 0$ and perfect detection $\sum_{mn\neq 10}\frac{F^2_{00,mn}}{F^2_{00,10}} = 0$, without considering the correlation term $\hbar k_m^2\mathrm{Re}\{\chi_m\}\cot\theta_a$, minimizing over N, we find that $S_\beta(f)_{min} = \hbar k_m^2|\chi_m|$ ($\theta = \pi/2$). And taking account of the correlation term $S_\beta(f)_{min} = \hbar k_m^2\mathrm{Im}\{\chi_m\}$ (θ not at $\pi/2$).

The cooperativity can be calculated as SNR of zero point motion to shot noise as

$$C = \frac{2PQ}{m_{eff}}\frac{kw_0^2k_m^2}{c\omega_m^2}$$

The calculation for classic noise is similar to that of quantum noise. The input field is $\hat{U}_{in} = \alpha(U_{00} + \frac{\Delta x(t)}{w_0}U_{10})$ assuming large classical noise and $\Delta x(t)$ is the displacement of the laser spot. Following the same procedures, we have

$$S_\beta(f) = \frac{S_{\Delta x}(f)/w_0^2}{N w_0^2 k^2 \sin^2\theta_a} |\cos\theta_a + 2\hbar D \chi_m \sin\theta_a|^2 + S_\beta^{th}(f),$$

and $S_\beta^{Cla}(\theta_a) = \frac{S_{\Delta x}(f)/w_0^2}{N w_0^2 k^2} \cot^2\theta_a$.